Crystal-field analysis of Eu^{3+} in Lu_2O_3

2003 J. Phys.: Condens. Matter 15 2169

(http://iopscience.iop.org/0953-8984/15/13/303)

INSTITUTE OF PHYSICS PUBLISHING JOURNAL OF PHYSICS: CONDENSED MATTER

J. Phys.: Condens. Matter **15** (2003) 2169–2181 PII: S0953-8984(03)57449-5

Crystal-field analysis of Eu^{3+} in Lu_2O_3

M Karbowiak[1,3], E Zych[1] and J Hölsä[2]

[1] Faculty of Chemistry, University of Wrocław, PL-50-383 Wrocław, 14 F. Joliot-Curie Street, Poland
[2] Department of Chemistry, University of Turku, FIN-20014 Turku, Finland

E-mail: karb@wchuwr.chem.uni.wroc.pl

Received 13 December 2002
Published 24 March 2003
Online at stacks.iop.org/JPhysCM/15/2169

Abstract

Low temperature (7 K) absorption spectra of polycrystalline sintered ceramic Lu_2O_3:Eu^{3+} were recorded between 3950 and 50 000 cm^{-1}. There are two different intrinsic Eu^{3+} sites, C_2 and S_6 (C_{3i}), in this host. A total of 105 crystal-field (CF) energy levels were assigned and fitted to a semiempirical Hamiltonian representing the combined free-ion (FI) and CF interactions for a $4f^6$ ion in the C_2 symmetry site. 10 FI and 14 CF parameters were varied simultaneously in the least square adjustments yielding an rms deviation between the calculated and experimental levels of 15 cm^{-1}. The CF strength parameter, S, obtained from calculated B_q^k parameters is larger for Lu_2O_3 when compared to the Y_2O_3 host, which is in accordance with the smaller ionic radius of the Lu^{3+} ion. The CF splittings of the $^7F_1$ and $^5D_1$ levels were also determined experimentally for the Eu^{3+} ion in the centrosymmetric S_6 site and the value of the second-rank B_0^2 CF parameter was calculated.

1. Introduction

Thorough crystal-field (CF) studies of lanthanide ions doped into Ln_2O_3 type host matrices based on analysis of absorption spectra are confined mainly to the yttrium oxide, Y_2O_3, lattice. In 1982 Chang *et al* [1] reported results of CF analysis of trivalent Kramers lanthanide ions in the C_2 site of Y_2O_3 single crystals. Applying a modified point charge CF model [2] they obtained a set of smoothly changing B_{km} CF parameters for the entire lanthanide series. Later on, Leavitt *et al* [3] extended the CF analysis to the non-Kramers lanthanide ions in the C_2 sites and obtained a set of phenomenological CF components A_{km} for this site. Results reported by Gruber *et al* [4] for the S_6 site completed the CF analysis of the Ln^{3+} ions in Y_2O_3. As far as we are aware no CF analysis has been performed for any Ln^{3+} ion in the Lu_2O_3 host taking into account the lines observed in low-temperature absorption spectra in the UV–vis and near-IR spectral regions. There are, however, some reports on the CF strength of Eu^{3+} in

[3] Author to whom any correspondence should be addressed.

the cubic Ln_2O_3 hosts (Ln = Sc, In, Lu, Y, Gd), restricted to the analysis of liquid nitrogen temperature emission spectra, thus taking into account only the levels of the low-lying ^7F_J ($J = 0$–4) multiplets [5, 6].

Lu_2O_3 is isostructural with Y_2O_3. It adopts a cubic C-type structure, space group $Ia3$ (T_h^7), in which each Lu^{3+} ion is surrounded by six oxygen ions located at corners of a cube [7, 8]. The lutetia lattice offers two crystallographically different lanthanide sites of C_2 and S_6 symmetry. The former is three times more abundant in the host than the latter. In the doped Lu_2O_3, the Eu^{3+} ions randomly substitute for Lu^{3+} in both the C_2 and S_6 sites [9]. The C_2 site possesses no centre of symmetry. Hence, the odd part of the CF potential mixes configurations of opposite parity into the 4f wavefunctions making the electric dipole transitions partially allowed within the 4f levels of the Eu^{3+} ions occupying the C_2 site. In contrast, for ions in the S_6 sites having inversion symmetry only magnetic dipole induced transitions, obeying the selection rule $\Delta J = 0, \pm 1$ (except $J = 0 \rightarrow 0$), are allowed. Thus, at liquid helium temperature for the Eu^{3+} ions occupying the S_6 site only absorption from the ground $^7F_0$ level to the two components (one doubly degenerate) of the $^5D_1$ multiplet can be expected.

The ionic radius of the Lu^{3+} host cation is smaller (0.861 Å) than that of Y^{3+} (0.900 Å), which is still smaller than that of Eu^{3+} (0.947 Å) [10]. Therefore, one could expect that in the Lu_2O_3 host the nearest surroundings will exert stronger influence on the Eu^{3+} ion than in the yttria host. The CF around the Eu^{3+} ion should, hence, be stronger in Lu_2O_3. Thus it is interesting to compare how this stronger CF influences the position of the barycentres, the splitting of SLJ multiplets and the values of CF parameters.

In our previous papers we have presented luminescence and site-selective excitation spectra of Eu^{3+} in the Lu_2O_3 host [9, 11, 12]. This paper reports the low-temperature optical absorption spectra recorded for a polycrystalline sintered semitransparent ceramic sample of Lu_2O_3:Eu^{3+} and results of calculations of 20 free-ion (FI) and 14 B_q^k CF parameters for Eu^{3+} in the C_2 site. Some basic analyses will be presented for the energy level scheme of the Eu^{3+} ions occupying the S_6 site, too.

2. Experimental details

The investigated sample was obtained in the form of a sintered disc 10 mm in diameter and about 0.5 mm thick. The powder for sintering was prepared using the combustion technique, the details of which have been given in a few earlier papers [11–13]. The appropriate mixture of $Lu(NO_3)_3{\cdot}5H_2O$ and $Eu(NO_3)_3{\cdot}6H_2O$ and glycine was dissolved in a small amount of water. Afterwards, the solution was dried at 140 °C and the solid residue was transferred into a furnace preheated to 650 °C. A vigorous reaction took place, shortly resulting in a formation of voluminous white powder of Lu_2O_3:Eu^{3+}. The powder was pressed under 9 tons of load and sintered in vacuum at 1650 °C for 5 h. The resulting semitransparent disc was optically polished and in such a form was used in measurements. The nominal Eu^{3+} content was 1 mol% with respect to Lu^{3+}.

For the low-temperature absorption measurements the sample was mounted in a liquid helium Oxford Instruments optical cryostat and cooled to 7 K. Unpolarized absorption spectra were recorded on a Cary 5 UV–vis–NIR spectrophotometer in the 3950–50 000 cm^{-1} (2530–200 nm) range.

3. Energy level calculations: theory

The energy level calculations were carried out applying the effective operator model [14–16]. The complete Hamiltonian includes the following terms:

$$\hat{H} = \hat{H}_{FI} + \hat{H}_{CF}. \tag{1}$$

$\hat{H}_{FI}$ contains the isotropic (FI) parts of $\hat{H}$ and is defined as

$$\hat{H}_{FI} = E_{ave} + \sum_{k=0,2,4,6} F^k(nf, nf)\hat{f}_k + \zeta_{4f}\hat{A}_{SO} + \alpha\hat{L}(\hat{L}+1) + \beta\hat{G}(G_2) + \gamma\hat{R}(R_7) + \sum_{i=2,3,4,6,7,8} T^i\hat{t}_i + \sum_{j=0,2,4} M^j\hat{m}_j + \sum_{k=2,4,6} P^k\hat{p}_k \quad (2)$$

where E_{ave} is the spherically symmetric one-electron part of the Hamiltonian, $F^k(nf, nf)$ (Slater integrals) and ζ_{4f} (spin–orbit coupling constant) represent the radial parts of the electrostatic and spin–orbit interactions, while f_k and A_{SO} are the angular parts of these interactions, respectively. The parameters α, β and γ are associated with the two-body correction terms. $G(G_2)$ and $G(R_7)$ are the Casimir operators for the G_2 and R_7 groups. L is the total orbital angular momentum. The three-particle configuration interaction is expressed by $T^i t_i$ ($i = 2, 3, 4, 6, 7, 8$), where T^i are parameters and t_i are three-particle operators. The electrostatically correlated spin–orbit perturbation is represented by the P^k parameters and those of the relativistic spin–spin and spin–other-orbit corrections by the M^j parameters. The operators associated with these parameters are designated by m_j and p_k, respectively. The $\hat{H}_{CF}$ term of the Hamiltonian represents the one-electron CF interactions and is defined as [14, 17]

$$\hat{H}_{CF} = \sum_i \sum_k \left\{ B_0^k \hat{C}_0^{(k)}(i) + \sum_{q=1}^{k} [\mathrm{Re}\, B_q^k (\hat{C}_q^{(k)}(i) + (-1)^q \hat{C}_{-q}^{(k)}(i)) + \mathrm{Im}\, B_q^k i(\hat{C}_q^{(k)}(i) - (-1)^q \hat{C}_{-q}^{(k)}(i))] \right\} \quad (3)$$

where i runs over all unpaired electrons of the unfilled 4f shell of the metal ion, k and q over all effective q components of the spherical tensor operator of rank $k(C_q^{(k)}(i))$ and B_q^k are the CF parameters. For the C_2 symmetry, the CF Hamiltonian includes 14 real and imaginary CF parameters, Re B_q^k and Im B_q^k, respectively—see table 1. The coordinate system was assumed to rotate around the C_2 axis in a way that the B_2^2 parameter is real.

CF calculations were performed by applying the f-shell empirical program written by Reid [18], running on a PC under the Linux Mandrake operating system. The eigenvectors and eigenvalues of the CF levels were obtained by the diagonalization of the combined FI and CF energy matrices. Due to the large matrix (3003×3003 elements) which would have to be handled for the $4f^6$ configuration, the basis set of 295 states was truncated to 90, which corresponds to the maximum energy of about 50 000 cm^{-1}. However, the matrix elements of the CF Hamiltonian were obtained from the wavefunctions associated with the intermediate-coupling diagonalization of the FI Hamiltonian (equation (2)), with parameter values taken from [19]. This procedure allows the inclusion of the effects of J mixing.

4. Results and discussion

4.1. Analysis of spectra: C_2 site

The absorption spectra of Lu_2O_3:Eu^{3+} sintered ceramic were recorded at 7 K in the 3950–50 000 cm^{-1} region. However, the intraconfigurational f–f transitions within Eu^{3+} ions can be observed up to about 37 500 cm^{-1} only. Above this energy a strong, broad ligand-to-metal charge transfer (CT) band appears hiding the much weaker 4f–4f transitions, and above about 45 000 cm^{-1} the fundamental absorption of the host is present [20].

Figure 1 presents the absorption transitions from the ground $^7F_0$ state to the excited $^5D_0$, $^5D_1$ and $^5D_2$ multiplets. In the $^7F_0 \rightarrow {}^5D_0$ transition region one dominant peak is observed at 17 216 cm^{-1} together with a very weak line at 17 241 cm^{-1}. Clearly, the stronger line originates

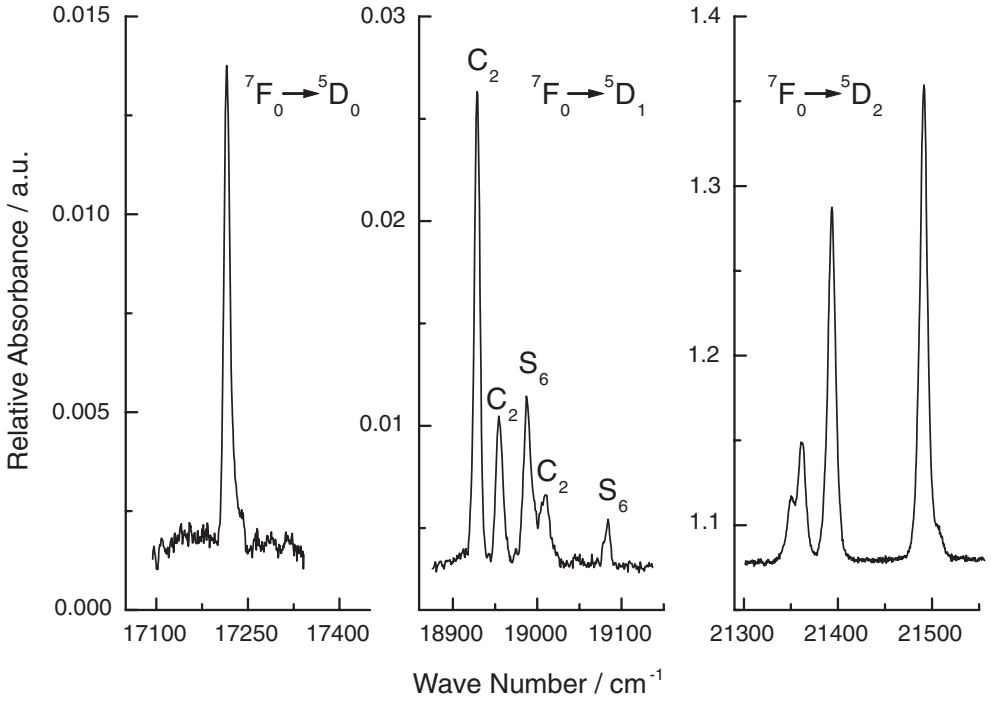

Figure 1. 7 K absorption spectrum of Lu_2O_3:Eu^{3+} in the $^7F_0 \rightarrow {}^5D_0$, $^7F_0 \rightarrow {}^5D_1$ and $^7F_0 \rightarrow {}^5D_2$ transition regions.

Table 1. FI and CF parameters for Lu_2O_3:Eu^{3+}.

Parameter[a]	Fitted value[b] (cm^{-1})	Parameter[a]	Fitted value[b] (cm^{-1})
E_{avg}	63 036(18)	B_0^4	−1557(27)
F^2	81 098(35)	B_2^4	−1633(25)
F^4	58 141(53)	Im B_2^4	242(45)
F^6	43 085(48)	B_4^4	798(41)
α	20.5(2.6)	Im B_4^4	−790(42)
β	−623(22)	B_0^6	685(34)
γ	1418(29)	B_2^6	−41(29)
ζ	1335(5)	Im B_2^6	91(42)
M^0	2.34(2.31)	B_4^6	635(85)
P^2	227(36)	Im B_4^6	−375(42)
B_0^2	−263(23)	B_6^6	142(43)
B_2^2	−756(17)	Im B_6^6	−385(33)
		rms	15
		n	105

[a] The T^k parameters were kept constant during the fitting procedure at the following values: $T^2 = 370$, $T^3 = 40$, $T^4 = 40$, $T^6 = -330$, $T^7 = 380$ and $T^8 = 370$ cm^{-1} [19]. The M^2, M^4, P^4 and P^6 parameters were constrained by the ratios $P^4/P^2 = 0.75$, $P^6/P^2 = 0.50$, $M^2/M^0 = 0.56$ and $M^4/M^0 = 0.38$ [22].
[b] The values in brackets are the estimated standard deviations of the parameters.

from the Eu^{3+} located in the noncentrosymmetric C_2 site. The appearance of the weak satellite peak is confusing, however. Its very low intensity alerts us that this could possibly result from

the formally forbidden $^7F_0 \rightarrow {}^5D_0$ absorption of the Eu^{3+} located at S_6 centrosymmetric site. Such an option we shall discuss later, on analysing the site S_6. Another possibility is that some of the dopant ions form pairs. This would result in a slightly different location of such ions' energy levels since the different ionic radii of Lu^{3+} and Eu^{3+} would necessarily distort the surroundings if such a Eu^{3+}–Eu^{3+} pair appears. Analogous line splitting due to pair formation was found in the case of Y_2O_3:Eu^{3+} 0.5% [21]. The effect was, however, much smaller, just about 5 cm^{-1} compared to about 25 cm^{-1} in our case. It is hard to believe that such a large difference could appear replacing Y^{3+} with only slightly smaller Lu^{3+}. Thus the origin of the weak line at 17 241 cm^{-1} remains unclear, unfortunately.

In the $^7F_0 \rightarrow {}^5D_2$ transition region there are four relatively strong lines clearly resolved and a very weak feature located at 21 508 cm^{-1} and superimposed on the line peaking at 21 491 cm^{-1}. We included the weak peak in the calculations, but in the final steps of the fitting procedure, since the calculations yielded a level close to the corresponding weak line. The $^7F_0 \rightarrow {}^5D_2$ hypersensitive transitions are much more intense compared to other intraconfigurational f–f absorption lines which feature is characteristic to all Ln_2O_3:Eu^{3+} spectra.

As expected, the situation is different in the region of the $^7F_0 \rightarrow {}^5D_1$ transitions where five lines can be easily identified. Obviously, two of them must necessarily result from the $^7F_0 \rightarrow {}^5D_1$ magnetic dipole induced transitions within the Eu^{3+} ions occupying the centrosymmetric S_6 site. The lines observed in this region have been separated utilizing site selective excitation [9, 12] and the assignment is indicated in figure 1.

The three weak lines observed at 24 254, 24 284 and 24 353 cm^{-1} (figure 2) should be assigned to $^7F_0 \rightarrow {}^5D_3$ transitions. They are forbidden by the selection rules for the induced electric dipole transitions, because $|\Delta J = 3|$, but their presence in the absorption spectrum indicates a relatively strong J-mixing for the Eu^{3+} ions in the Lu_2O_3 host. Figure 2 also presents transitions to the $^5L_6$ multiplet and 11 nicely resolved lines out of 13 allowed by theory could be easily observed. In the higher energy region the transitions to ^5G_J ($J = 2$–6) multiplets overlap and could not be unambiguously assigned (figure 3). The LSJ numbers ascribed to those transitions resulted from CF calculations. The four peaks observed in the 27 450–27 630 energy range (see the inset in figure 2) were assigned to the $^7F_0 \rightarrow {}^5D_4$ transitions. Several lines observed at higher energies were assigned to transitions to the CF levels of the ^5H_J, ^5F_J, ^5I_J and ^5K_J multiplets with the aid of CF calculations.

The lowest energy lines we could observe in the 3950–4350 cm^{-1} region of absorption spectra result from the $^7F_0 \rightarrow {}^7F_5$ transitions. Above them, the $^7F_0 \rightarrow {}^7F_6$ absorption lines are observed in the 4790–5700 cm^{-1} region. The energy levels of lower positioned levels of ^7F_J multiplets have been determined from the luminescence spectra [9, 12]. Altogether, 105 energy levels observed in the absorption and luminescence spectra were assigned and included in the fitting procedure.

4.2. Energy level calculations

The FI and B_q^k parameters of the semiempirical Hamiltonian (equations (1)–(3)) were determined by minimizing the difference between the energies of the experimental and calculated CF levels by the least squares method. It is not possible to label the CF levels with irreducible representations from unpolarized measurements on polycrystalline samples. Therefore, within a given multiplet, subsequent experimental levels were assigned to the energetically closest calculated one. As we have already mentioned, the initial values of the FI parameters were taken from [19] and as the initial B_q^k parameters the values obtained by Leavitt *et al* [3] for Eu^{3+} in Y_2O_3 were applied. At the beginning of the fitting procedure we

Table 2. Calculated and experimental energy levels for $Lu_2O_3:Eu^{3+}$ (the C_2 site).

$^{2S+1}L_J$ [a]	Energy[b] (cm^{-1}) Calc	Exp	$E_{exp} - E_{calc}$ (cm^{-1})	$^{2S+1}L_J$ [a]	Energy[b] (cm^{-1}) Calc	Exp	$E_{exp} - E_{calc}$ (cm^{-1})
$^7F_0$	−10	0	10		18 946	18 955	9
$^7F_1$	205	186	−19		19 021	19 010	−11
	358	364	6	$^5D_2$	21 367	21 350	−17
	554	555	1		21 379	21 362	−17
$^7F_2$	856	856	0		21 393	21 393	0
	865	899	34		21 467	21 491	24
	919	951	32		21 494	21 508	14
	1 192	1 197	5	$^5D_3$	24 228	—	—
	1 393	1 397	4		24 249	24 254	5
$^7F_3$	1 841	1 837	−4		24 274	—	—
	1 877	1 860	−17		24 288	24 284	−4
	1 904	1 904	0		24 291	—	—
	1 949	—	—		24 329	—	—
	2 018	2 031	13		24 340	24 353	13
	2 139	—	—	$^5L_6$	24 575	24 585	10
	2 156	2 153	−3		24 620	24 622	2
$^7F_4$	2 665	2 672	7		24 642	—	—
	2 757	—	—		24 683	24 664	−19
	2 806	2 812	5		24 708	24 694	−14
	2 993	—	—		24 753	24 747	−6
	3 048	3 022	−26		24 914	24 920	6
	3 099	3 084	−15		25 096	25 102	6
	3 146	3 131	−15		25 245	—	—
	3 183	3 201	18		25 268	25 251	−17
	3 232	—	—		25 328	25 309	−19
$^7F_5$	3 757	—	—		25 357	25 396	38
	3 804	—	—		25 401	25 432	31
	3 828	—	—	$^5L_7$ [c]	25 720	25 700	−20
	3 919	—	—	$+ {}^5L_8$	25 741	25 740	−1
	3 925	—	—	$+ {}^5G_J$	25 790	25 788	−2
	3 958	3 959	1		25 900	25 919	19
	4 011	4 031	20		25 957	25 958	−1
	4 201	—	—		26 057	26 060	3
	4 224	—	—		26 136	26 141	5
	4 282	—	—		26 192	26 186	−6
	4 341	—	—		26 211	26 215	4
$^7F_6$	4 790	4 796	6		26 299	26 294	−5
	4 796	4 815	19		26 332	26 337	5
	5 027	—	—		26 395	26 396	1
	5 033	—	—		26 443	26 447	4
	5 054	5 052	−2		26 517	26 521	4
	5 087	5 065	−22		26 582	26 582	0
	5 305	—	—		26 696	26 690	−6
	5 333	5 327	−6		26 732	26 747	15
	5 342	—	—		26 794	26 791	−3
	5 475	—	—		26 912	26 911	−1
	5 477	5 483	6		27 010	27 021	11
	5 677	5 668	−9		27 039	27 055	16
	5 678	—	—		27 300	27 305	5
$^5D_0$	17 224	17 216	−9	$^5D_4$ [d]	27 477	27 457	−20
$^5D_1$	18 914	18 929	14		27 496	—	—

Table 2. (Continued.)

$^{2S+1}L_J$[a]	Energy[b] (cm^{-1}) Calc	Exp	$E_{exp} - E_{calc}$ (cm^{-1})	$^{2S+1}L_J$[a]	Energy[b] (cm^{-1}) Calc	Exp	$E_{exp} - E_{calc}$ (cm^{-1})
	27 500	27 502	2		33 145	33 142	−3
	27 541	—	—	$^5F_4$	33 187	33 192	5
	27 554	27 551	−3		33 209	—	—
	27 561				33 230	33 228	−2
	27 567	—	—		33 236	—	—
	27 596	27 624	28		33 277	33 258	19
	27 680				33 283	33 288	5
^5H_J[e]	30 592	30 608	16		33 301	—	—
	30 806	30 804	−3		33 313	33 316	3
	30 881	30 879	−2		33 320	33 341	21
	30 929	30 932	3	$^5F_5$[f]	33 585	33 592	7
	30 969	30 964	−5	$+ {}^5I_{4-8}$	33 658	33 657	−1
	30 999	31 003	4		33 719	33 712	−7
	31 032	31 040	8		33 844	33 854	10
	31 216	31 204	−12		34 315	34 290	−25
	31 275	31 273	−2		34 347	34 356	−9
	31 317	31 304	−13		34 422	34 430	8
	31 404	31 413	9		34 460	34 453	−7
$^5F_2$	32 577	32 557	−20		34 598	34 591	−7
$+ {}^5F_3$	32 578	32 577	−1		34 666	34 645	−21
$+ {}^3P_0$	32 644	32 628	−16	^5K_J[g]	35 810	35 813	3
	32 653	—	—		35 868	35 856	−12
	32 682	—	—		36 892	36 895	3
	32 747	—	—		36 949	36 941	−8
	32 748	—	—		37 002	37 002	0
	32 783	—	—		37 122	37 155	33
	32 812	32 814	2		37 814	37 802	−12
	32 835	32 841	5		37 873	37 873	0
	32 851	—	—		37 949	37 943	−6
	32 889	—	—		38 027	38 033	6
	32 934	32942	8		38 120	38 127	7
$^5F_1$	33 071	33 074	3		38 199	38 174	−25
	33 092	33 107	15				

[a] Main FI component quantum numbers for the state associated with the group.
[b] Calculated with the best-fit FI and CF parameters of table 1.
[c] 77 energy levels belonging to $^5L_7$, $^5L_8$ and ^5G_J ($J = 2$–6) states are calculated in this energy region. In the table we included only those for which experimental energy levels are assigned (22 levels).
[d] 49 energy levels belonging to $^5D_4$, $^5L_9$ and $^5L_{10}$ states are calculated. Only four assigned as transitions to the $^5D_4$ multiplet are observed and included in the table together with theoretical energy values calculated for this multiplet. The rest of the calculated levels are omitted from the table.
[e] 11 experimental levels from among 55 predicted by theory were assigned in the ^5H_J ($J = 3$–7) energy region, and only these are included in the table.
[f] 76 energy levels belonging to $^5F_5$ and ^5I_J ($J = 4$–8) multiplets are calculated in this energy region. In the table we included only those ten levels for which experimental energy levels are assigned.
[g] 11 experimental energy levels were assigned for ^5K_J levels.

included only those levels which could be assigned unambiguously (51 energy levels). These include the Stark levels of the ^7F_J ($J = 0$–6) and ^5D_J ($J = 0$–3) multiplets as well as the CF levels of the $^5L_6$ multiplet. At this step a set of the electron repulsion parameters (F^2, F^4, F^6),

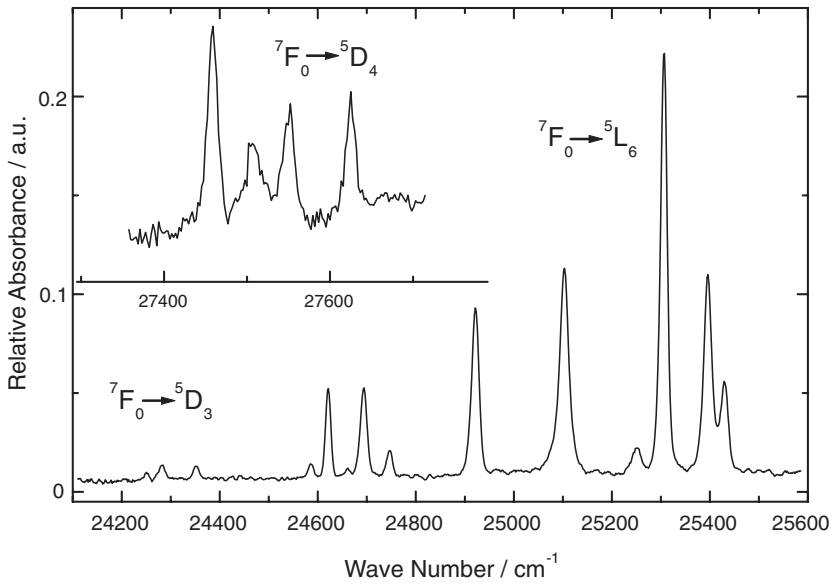

Figure 2. 7 K absorption spectrum of Lu_2O_3:Eu^{3+} showing transitions from the $^7F_0$ ground level to the $^5D_3$ and $^5L_6$ multiplets. The inset presents the $^7F_0 \rightarrow {}^5D_4$ transition region.

the spin–orbit coupling constant ζ_{4f} and 14 B_q^k parameters were adjusted. Additional energy levels were included in the fit and remaining FI Hamiltonian parameters were relaxed one after the other as the iteration procedure proceeded. In the final step of the least squares procedure the 14 CF B_q^k parameters as well as 10 FI parameters were freely varied. The values obtained for the best fit are included in table 1. The T^k three-body interaction parameters were fixed at constant values [19] in all steps. The P^4, P^6, M^2 and M^4 parameters were constrained by the pseudo-relativistic Hartree–Fock ratios: $P^4/P^2 = 0.75$, $P^6/P^2 = 0.50$, $M^2/M^0 = 0.56$ and $M^4/M^0 = 0.38$ [22]. All adjusted parameters achieved stable values at the end of the fitting procedure and reached physically acceptable values. The errors of individual parameters are also relatively low. The only exception is the M^0 for which the error reaches the parameter value. Nevertheless, the value itself stays reasonable. The experimental and calculated energy levels are presented in table 2. In this table we do not include multiplets for which experimental levels were not observed. The calculated values of these levels can be easily generated from the parameter values presented in table 1. The goodness of the fit can be judged by the root mean square deviation, rms, value, which is defined as follows:

$$\mathrm{rms} = \left[\frac{\sum_{i=1}^{n} (E_{\mathrm{exp}}(i) - E_{\mathrm{calc}}(i))^2}{(n-p)}\right]^{1/2} \tag{4}$$

where n is equal to the number of experimental levels and p is the number of parameters that are varied freely. The rms value for the final fit was 15 cm^{-1}. Only for two levels, observed at 25 396 and 25 432 cm^{-1}, and assigned to the $^5L_6$ manifold, are there relatively large discrepancies between the calculated and experimental energies, equal to 38 and 31 cm^{-1}, respectively. Nevertheless, any other assignment would lead to even larger discrepancy between the experimental and calculated values. Thus the assignment of the relatively strong distinct lines (figure 2) seems to be reasonable.

Unfortunately, we cannot compare calculated values of FI parameters for Eu^{3+} in Lu_2O_3 with those in Y_2O_3. The reason is that for yttria these parameters have not been adjusted in

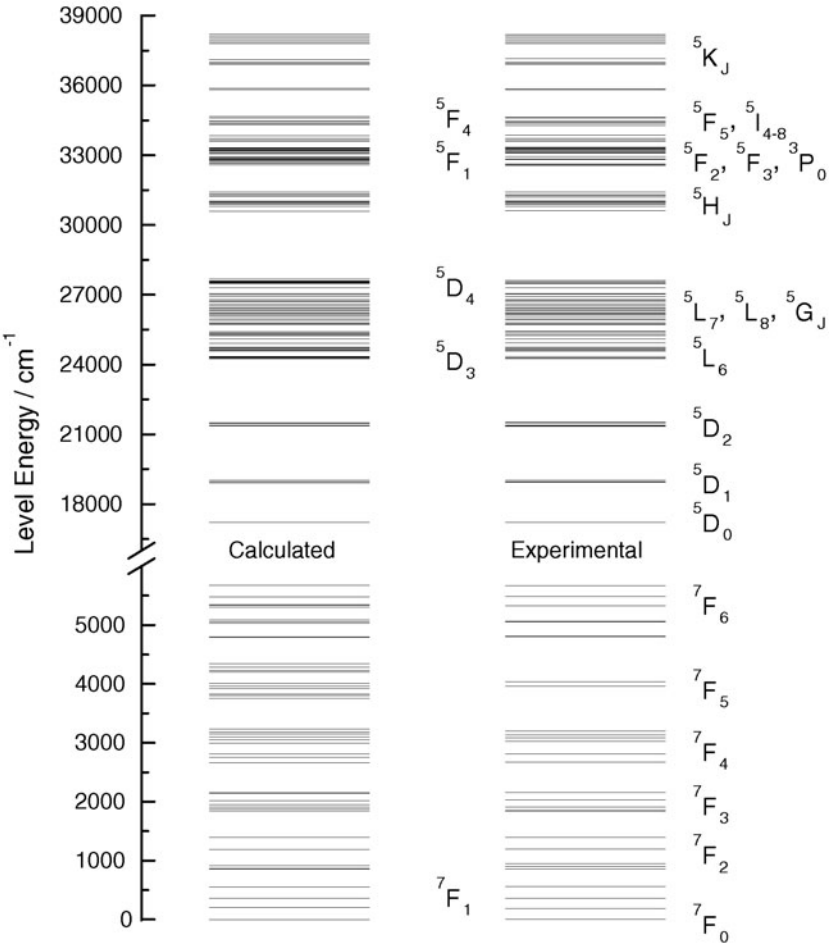

Figure 3. Experimental and simulated energy level schemes of Lu_2O_3:Eu^{3+} (the C_2 site).

analysis reported by Leavitt *et al* [3]. Nevertheless, the F^k electron repulsion parameters, the spin–orbit coupling constant ζ_{4f}, as well as the configuration interaction parameters α, β and γ obtained in our analysis fall within the values typical for the Eu^{3+} ion [23]. The M^0 parameter is calculated, as we have already mentioned, with relatively large error, close to the parameter value. However, the value still seems to be reliable and does not deviate from those previously determined for other hosts. The rms value could be decreased to about 10 cm^{-1} if we allowed the T^k parameter to be varied in the fitting procedure. Unfortunately, the resulting T^k parameters deviate considerably from the mean values obtained for Eu^{3+} in other hosts and they seem to have poor physical meaning. This results from the fact that the three-particle configuration interaction parameters show a great sensitivity to only a few chosen $^{2S+1}L_J$ levels, often to those located at the high energy range of the $4f^6$ configuration. These levels were not observed in our experiment since the low-lying CT band of Eu^{3+} overlaps them, so we constrained the T^k parameters to the literature values [19]. It seems, however, that the inclusion of the FI parameters in the fitting procedure is, at least partially, responsible for the present rms value. This explains the better fit (rms was 10 cm^{-1} for 51 experimental energy levels belonging to the ^7F_J ($J = 0$–6) and ^5D_J ($J = 0$–3) multiplets) obtained by Leavitt

et al [3] for Y_2O_3:Eu^{3+} as compared to our analysis. However, in their FI Hamiltonian the authors applied the values of parameters appropriate for Eu^{3+} in aqueous solution and used the *centroid parameters* (corresponding to the experimental centres of gravity of the CF split levels, if J mixing is neglected) for artificial adjustment of the multiplet barycentres. The *centroid parameters* allowed for individual adjustment of calculated multiplet barycentres to experiment, and thus deviations caused by inadequacy in FI determination are eliminated.

The present values for the B_q^k parameters may be compared to those reported by Leavitt *et al* [3] for Y_2O_3:Eu^{3+} and by Antic-Fidancev *et al* [6] for different Ln_2O_3:Eu^{3+}. In the latter analysis, since the experimental data were restricted to only 21 CF levels of the $^7F_{0-4}$ multiplets, the reliability of the sixth-rank parameters is lower than that of the second- and fourth-rank parameters. The values of our second-rank parameters, B_q^2, are in accordance with those reported both by Leavitt *et al* [3] and Antic-Fidancev *et al* [6]. The same is true for the fourth-rank parameters, except for Im B_4^4. In our analysis we obtained Im $B_4^4 = -790$ cm^{-1}, which is very close to the -780 cm^{-1} reported by Leavitt *et al* [3]. The calculations performed by Antic-Fidancev *et al* [6] produced the value of 448 cm^{-1}.

For the sixth-rank parameters the only larger differences between the present results and those of Leavitt *et al* [3] are observed for the Re B_2^6, Im B_2^6 and Im B_6^6 parameters. The absolute value of the Im B_6^6 resulting from our analysis (-385 cm^{-1}) is similar to that found by Antic-Fidancev *et al* [6] (261 cm^{-1}) but considerably larger than obtained for Y_2O_3:Eu^{3+} (-35 cm^{-1}). This may simply reflect a stronger CF felt by the Eu^{3+} ions in Lu_2O_3. In the case of the B_2^6 and Im B_2^6 parameters we have obtained smaller absolute values of -41 and 91 cm^{-1} as compared to 159 and -198 cm^{-1} in Y_2O_3, for the real and imaginary parts, respectively. Antic-Fidancev *et al* [6] obtained for these parameters values of 458 and 222 cm^{-1}. In the CF analyses for other Ln^{3+} ions in Y_2O_3 the values obtained for the Im B_2^6 are not consistent. For example, negative Im B_2^6 values have been reported for Eu^{3+} (-198) and Nd^{3+} (-115 cm^{-1}), whereas positive ones for Tb^{3+} (68) and Er^{3+} (119 cm^{-1}) [1, 3]. In general, it is difficult to determine accurately the values of B_q^6 parameters. They depend mainly on the CF splitting of states with $J > 3$. The splitting of each level with $J > 3$ is also a function of second- and fourth-rank parameters. Moreover, for states with $J > 3$ the number of CF levels observed experimentally for the Eu^{3+} ion is usually lower than predicted by theory, due to the low intensity of some of the transitions. Thus the assignment of experimental levels to calculated ones is to some degree equivocal.

4.3. Crystal field strength

Due to the difference in ionic radii, the CF is expected to affect the Eu^{3+} ions more strongly in the Lu_2O_3 than in the Y_2O_3 host. This is reflected first of all by differences in the total CF splitting of the $^{2S+1}L_J$ multiplets. In the case of the Lu_2O_3 host the splitting of 369 and 81 cm^{-1} was determined for the $^7F_1$ and $^5D_1$ multiplets, compared to 344 and 62 cm^{-1} determined for Y_2O_3 [3], respectively. To describe the CF splitting of states with $J = 1$ second-rank CF parameters are required, i.e. B_0^2 and B_2^2 for the C_2 symmetry. According to Leavitt *et al* [3] the S^2 CF strength parameter may be calculated from the simple formula [24]

$$S^2 = \left[\frac{1}{(2 \times 2 + 1)}\left(|B_0^2|^2 + 2\sum_{q>0}|B_q^2|^2\right)\right]^{1/2}. \tag{5}$$

This gives 492 and 484 cm^{-1} for the Lu_2O_3 and Y_2O_3 hosts, respectively. Thus the trend in magnitude is maintained, but the difference in S^2 is smaller than the differences in experimental splittings of multiplets with $J = 1$ determined for Lu_2O_3 and Y_2O_3. For Y_2O_3:Eu^{3+} the calculated splittings of the $^7F_1$ and $^5D_1$ multiplets (356 and 104 cm^{-1},

respectively) are considerably larger than the experimental ones (344 and 62 cm^{-1}). In our results for Lu_2O_3:Eu^{3+} this discrepancy is smaller, and the calculated values are 349 and 107 cm^{-1} as compared to the experimental values of 369 and 81 cm^{-1} for the $^7F_1$ and $^5D_1$ multiplets, respectively. Hence, we feel that B_q^2 parameters reported by Leavitt *et al* [3] for Y_2O_3 ($B_0^2 = -276$ and $B_2^2 = -740$ cm^{-1}) are slightly overestimated. This conclusion is supported by the results reported recently by Antic-Fidancev *et al* [6] for the CF analysis conducted on the basis of the $^7F_{0-4}$ CF levels. For Y_2O_3:Eu^{3+} these authors found the values of -253 and -651 cm^{-1} for B_0^2 and B_2^2, respectively. The parameter S^2 calculated from those B_q^2 values is equal to 427 cm^{-1}. This value is 13% smaller than found by us for Lu_2O_3 and corresponds nicely to the observed differences in the CF splitting of the $^7F_1$ and $^5D_1$ multiplets for Lu_2O_3 and Y_2O_3.

The differences in the CF strength in both hosts can be expressed in a better manner by the overall CF strength parameter defined as [24]:

$$S = \left\{ \tfrac{1}{3} \sum_k \frac{1}{(2k+1)} \left(|B_0^k|^2 + 2 \sum_{q>0} (|\mathrm{Re}\, B_q^k|^2 + |\mathrm{Im}\, B_q^k|^2) \right) \right\}^{1/2}. \tag{6}$$

The value of S for Lu_2O_3:Eu^{3+} is equal to 718 cm^{-1} whereas for Y_2O_3:Eu^{3+} it is 673 cm^{-1} [3]. The difference in the CF strength is about 6% and is only slightly larger than the difference in ionic radii of host cations (4.5%) [10]. The S value (762 cm^{-1}) resulting from the analysis reported by Antic-Fidancev *et al* [6] for Lu_2O_3:Eu^{3+}, but carried out on the basis of the $^7F_{0-4}$ CF levels, is still larger than obtained in the present analysis. This value seems to be too high, which is also evident from figure 4 presented in [6], which describes the dependence of the CF strength on the ionic radius of the Ln^{3+} host cation for the Ln_2O_3:Eu^{3+} (Ln = Sc, In, Y, Gd) series. The S value obtained for Lu_2O_3:Eu^{3+} is the only one which deviates significantly towards a higher value from the linear relationship.

4.4. Analysis of spectra: S_6 site

When the Eu^{3+} ions occupy the S_6 sites in the Lu_2O_3 host only two $^7F_0 \rightarrow {}^5D_1$ transitions are allowed in absorption. Indeed, we found the expected two lines in the appropriate part of the absorption spectrum (figure 1). The energies of the CF components of the $^5D_1$ multiplet determined from the absorption and excitation spectra are equal to 18 979 and 19 074 cm^{-1}. According to the traditional assignment presented for Y_2O_3:Eu^{3+} [4, 25, 26], the higher CF level is a singlet level. However, the present interpretation [27], supported by theoretical calculations [28], gives a reversed order, i.e. the degenerate CF level is the higher one. Since the $^5D_1$ CF level energies are very similar for both oxide hosts, the latter assignment is adopted.

A slightly different situation could be expected in the emission. The selection rule $\Delta J = 0, 1$ (but no $J = 0 \rightarrow 0$ transition) gave hope for recording not only the $^5D_0 \rightarrow {}^7F_1$ transition, which we easily found and separated from analogous emission lines of Eu^{3+} in the C_2 site [9, 12], but also for the $^5D_1 \rightarrow {}^7F_{0,1}$ transitions. Although we analysed spectra for various concentrations of the dopant the emission from the $^5D_1$ multiplet could only be assigned to the Eu^{3+} ions occupying the C_2 site. The very weak line on the high energy side of the $^7F_0 \rightarrow {}^5D_0$ transition (figure 1) could possibly result from the (formally forbidden) $^7F_0 \rightarrow {}^5D_0$ for Eu^{3+} in the S_6 site. However, this idea had to be rejected because of an unreasonably small energy gap between the $^7F_0$ and $^5D_0$ levels for the S_6 site as compared to the Y_2O_3 host [4, 21].

The last chance to obtain the $^5D_0$ level energy needed was given by the careful analysis of the energy gap between the $^5D_0$ level and $^5D_1$ barycentre. Since this energy gap is exclusively determined by the spin–orbit coupling constant, one will readily obtain the $^5D_0$ level energy

Table 3. Calculated and experimental energy levels for Lu_2O_3:Eu^{3+} (the S_6 site).

$^{2S+1}L_J$ [a]	Level	E_{calc} [b] (cm^{-1})	E_{exp} (cm^{-1})
$^7F_0$	A_g	0	0
$^7F_1$	A_g	110	110
	E_g	402	401
$^5D_0$	A_g	17 283	17 283
$^5D_1$	A_g	18 980	18 979
	E_g	19 068	19 070

[a] Nominal quantum numbers for the atomic state associated with the group.
[b] Calculated with B_0^2 CF parameter equal to $-1032\ cm^{-1}$.

from the $^5D_1$ barycentre using statistical analysis of the energy level schemes of Eu^{3+} ions in different hosts [23, 27]. Such an analysis was used with success for Y_2O_3:Eu^{3+} and resulted in an accurate reinterpretation of the S_6 energy level scheme. The $^5D_0$ level corresponding to the $^5D_1$ barycentre at 19 042 cm^{-1} (19 050 for Y_2O_3:Eu^{3+}) was found at 17 283 cm^{-1} (17 302 cm^{-1} for Y_2O_3:Eu^{3+}). These values, though very similar, are consistent with the nephelauxetic effect in the Ln_2O_3 series. Finally, the reinvestigation of the high temperature excitation spectrum of the $^5D_0 \rightarrow {}^7F_1$ transition (at 582.8 nm) in the $^7F_{0,1} \rightarrow {}^5D_1$ transition range (between 523 and 528 nm) revealed superimposed lines due to the very similar energy separation of the lowest CF component of $^7F_1$ and $^7F_0$ and the two CF components of the $^5D_1$ multiplet. The energy level schemes for the $^7F_{0,1}$ and $^5D_{0,1}$ multiplets were thus determined unambiguously (table 3).

The CF splitting of the $^7F_1$ and $^5D_1$ multiplets is described by only one CF parameter, B_0^2. It is not possible to determine values of the FI Hamiltonian knowing barycentres of only two multiplets. Therefore we assumed for the FI Hamiltonian the same parameters as obtained for the C_2 site, and we corrected the positions of the calculated barycentres of the $^7F_0$, $^7F_1$, $^5D_0$ and $^5D_1$ multiplets by treating them as independently adjustable parameters in the fit. In this way the value of $-1032\ cm^{-1}$ was determined for the B_0^2 parameter which is in accordance with 1172 cm^{-1} calculated for Y_2O_3 [4]—except for the sign, of course. It should be noted, however, that the other CF parameters which have non-negligible values according to the theoretical calculations [28] may affect the B_0^2 value. The B_0^2 value obtained must be considered as a preliminary one but a more accurate value is very difficult to obtain since the lack of experimental data on the CF splittings of the other multiplets.

5. Conclusions

The NIR–vis–UV absorption spectra at 7 K and CF analysis are reported for the Eu^{3+} ions in Lu_2O_3. 105 CF energy levels of the Eu^{3+} ions in the C_2 sites were determined from the luminescence and absorption spectra. The energy level scheme of the $4f^6$ configuration (for the C_2 site symmetry and below 50 000 cm^{-1}) was parametrized in terms of 20 FI and 14 CF parameters. A good agreement between the experimental and calculated energy level schemes was obtained with a rms deviation equal to 15 cm^{-1}. In the Lu_2O_3 host, the Eu^{3+} ion experiences a stronger CF than in Y_2O_3, as proved by the higher value of the CF strength parameter S.

For the Eu^{3+} ions in the S_6 sites, the CF splitting of the state as well as energy of CF levels of the $^7F_1$ and $^5D_1$ multiplets were determined from the site-selective emission and excitation spectra. The approximate value of the second-rank B_0^2 CF parameter was determined.

In order to further improve both the assignment of experimental levels and the accuracy of the calculation, measurements on a single crystal using polarized light would be necessary. Nevertheless, comparing our findings to those reported in literature for Eu^{3+} in other oxide hosts we can state that they are generally very reliable.

Acknowledgments

The Polish Committee for Scientific Research (KBN) is greatly acknowledged for the financial support of this work under grant 4 T09B 087 23. Dr E Antic-Fidancev (UMR 7574, CNRS ENSCP, Paris France) and Dr M Lastusaari (Department of Chemistry, University of Turku, Finland) are thanked for useful discussions during the preparation of the manuscript.

References

[1] Chang N C, Gruber J B, Leavitt R P and Morrison C A 1982 *J. Chem. Phys.* **76** 3877
[2] Morrison C A and Leavitt R P 1979 *J. Chem. Phys.* **71** 2366
[3] Leavitt R P, Gruber J B, Chang N C and Morrison C A 1982 *J. Chem. Phys.* **76** 4775
[4] Gruber J B, Leavitt R P, Morrison C A and Chang N C 1985 *J. Chem. Phys.* **82** 5373
[5] Malta O L, Antic-Fidancev E, Lemaitre-Blaise M, Milicic-Tang A and Taibi M 1995 *J. Alloys Compounds* **228** 41
[6] Antic-Fidancev E, Hölsä J and Lastusaari M 2002 *J. Alloys Compounds* **341** 82
[7] ICSD Collection Code No. 40471, FIZ Karlsruhe and Gmelin Inst. (1990) Release 99/1
[8] Saiki A, Ishizawa N, Mizutani N and Kato M 1984 *Acta Crystallogr.* B **40** 76
[9] Zych E 2002 *J. Phys.: Condens. Matter* **14** 5637
[10] Shannon R D 1976 *Acta Crystallogr.* A **32** 751
[11] Zych E, Hreniak D and Stręk W 2002 *J. Phys. Chem.* B **106** 3805
[12] Zych E, Karbowiak M, Domagala K and Hubert S 2002 *J. Alloys Compounds* **341** 381
[13] Zych E 2001 *Opt. Mater.* **16** 445
[14] Wybourne B G 1965 *Spectroscopic Properties of Rare Earths* (New York: Interscience)
[15] Carnall W T, Crosswhite H, Crosswhite H M, Hessler J P, Edelstein N M, Conway J G, Shalimoff G V and Sarup R 1980 *J. Chem. Phys.* **72** 5089
[16] Edelstein N M 1995 *J. Alloys Compounds* **223** 197
[17] Mulak J and Gajek Z 2000 *The Effective Crystal Field Potential* (Amsterdam: Elsevier)
[18] Reid M F University of Canterbury, New Zealand, private information
[19] Richardson F S, Reid M F, Dallara J J and Smith R D 1985 *J. Chem. Phys.* **83** 3813
[20] Zych E, Dereń P J, Stręk W, Meijerink A, Mielcarek W and Domagała K 2001 *J. Alloys Compounds* **323/324** 8
[21] Buijs M, Meijerink A and Blasse G 1987 *J. Lumin.* **37** 9
[22] Judd B R and Crosswhite H 1984 *J. Opt. Soc. Am.* B **1** 255
[23] Görller-Walrand C and Binnemans K 1996 Rationalization of crystal-field parametrization *Handbook on the Physics and Chemistry of Rare Earths* vol 23, ed K A Jr Gschneidner and Eyring LeRoy (Amsterdam: Elsevier) ch 155
[24] Leavitt R P, Gruber J B, Chang N C and Morrison C A 1982 *J. Chem. Phys.* **71** 1661
[25] Heber J, Hellwege K H, Köbler U and Murmann H 1970 *Z. Phys.* **237** 189
[26] Schaak G and Koningstein J A 1970 *J. Opt. Soc. Am.* **60** 1110
[27] Antic-Fidancev E, Hölsä J and Lastusaari M 2003 *J. Phys.: Condens. Matter* **15** 863
[28] Faucher M and Dexpert-Ghys J 1981 *Phys. Rev.* B **24** 3138